Astron. Astrophys. 326, 963–975 (1997)

ASTRONOMY
AND
ASTROPHYSICS

Gas and dust in the active spiral galaxy NGC 3079

J. Braine[1,2], **M. Guélin**[2], **M. Dumke**[3], **N. Brouillet**[1], **F. Herpin**[1], **and R. Wielebinski**[3]

[1] Observatoire de Bordeaux, URA 352, CNRS/INSU, B.P. 89, F-33270 Floirac, France
[2] Institut de Radioastronomie Millimétrique, 300 rue de la Piscine, F-38406 St. Martin d'Hères, France
[3] Max-Planck-Institut für Radioastronomie, Auf dem Hügel 69, D-53121 Bonn, Germany

Received 5 May 1997 / Accepted 16 June 1997

Abstract. We present detailed observations of the 1.2 mm continuum and the CO line emission in the exceptional starburst/active galaxy NGC 3079 with the IRAM 30-m telescope.

The 1.2 mm thermal dust emission is much less centrally concentrated than the CO or radio continuum. Roughly 10% of the total 1.2 mm flux comes from the central 11″ as opposed to $\sim 40\%$ for the CO or radio continuum.

We find no evidence for cool dust in the center of NGC 3079. A dust temperature of 32 K fits the data well. We then determine $N(\mathrm{H_2})/I_{\mathrm{CO(2-1)}} \approx 3 \times 10^{19}\,\mathrm{cm^{-2}(\,K\,km\,s^{-1})^{-1}}$, roughly an order of magnitude below most estimates.

In the disk, cool dust is present. For $T_{\mathrm{dust}} = 17\,\mathrm{K}$, the cross-section (or absorption coefficient) we derive for dust in the atomic medium is very close to the value of Draine & Lee (1984). The combination of the errors in the HI column density and the 1.2 mm thermal dust emission are probably less than a factor 2 in these and other recent observations. Unless the dust temperature has been severely overestimated, the dependence of the dust opacity on wavelength (λ) is closer to λ^{-2} than $\lambda^{-1.5}$ between 100 μm and 1.2 mm.

Based on this cross-section, we estimate an average conversion factor of $N(\mathrm{H_2})/I_{\mathrm{CO(2-1)}} \approx 1-2\times 10^{20}\,\mathrm{cm^{-2}(\,K\,km\,s^{-1})^{-1}}$ in the disk. This is within the range of estimates for our galactic disk, although lower than early estimates.

Given the very low $N(\mathrm{H_2})/I_{\mathrm{CO(2-1)}}$ value found for the nuclear region, we compare it with ratios derived from radiative transfer equations and ^{13}CO measurements. These estimates are in good agreement with our dust-based $N(\mathrm{H_2})/I_{\mathrm{CO}}$ factor. It appears unlikely that grain emission is enhanced (with respect to that in the atomic medium) through grain-grain agglomeration or through condensation of molecules onto grains.

The dust mantles may be partially evaporated in the center of NGC 3079. The dust temperature may allow evaporation of CO-rich mantles and C-shocks are another plausible mechanism capable of disrupting mantles while leaving CO molecules intact. The effect would be to raise the $N(\mathrm{H_2})/I_{\mathrm{CO(2-1)}}$ ratio slightly and to increase the gas-phase CO abundance.

Send offprint requests to: Jonathan Braine in Bordeaux,
braine@observ.u-bordeaux.fr

Key words: galaxies: individual: NGC 3079 — galaxies: starburst — galaxies: ISM — galaxies, nuclei — ISM: clouds

1. Introduction

Gas and dust are assumed to be so intimately mixed in interstellar space that dust emission and absorption are considered among the most reliable tracers of the atomic *and* molecular gas. More specifically, in standard interstellar clouds, the mm thermal emission from dust grains, which is optically thin, is proportional to the hydrogen column density, $N_{\mathrm{H}} = N(\mathrm{HI}) + 2N(\mathrm{H_2})$, and depends mildly on the dust grain temperature, and little on the grain sizes and mantle composition. The dust emission per H-atom is proportional to the metallicity because the grains are mostly composed of metals so the dust mass varies with Z while the metallicity does not affect the gas mass. As shown e.g. by Mezger et al. (1990), it can be expressed as:

$$\frac{S_\nu}{\Omega} \simeq \sigma_\lambda\, N_{\mathrm{H}}\, B(\nu, <T_d>) \tag{1}$$

$$\frac{S_\nu}{\Omega} \simeq N_{\mathrm{H}}\, B(\nu, <T_d>)\, b\, \frac{Z}{Z_\odot}\, \sigma_{\mathrm{mm}} \lambda_{\mathrm{mm}}^m \tag{2}$$

where $<T_d>$ is the average dust temperature, $Z/Z_\odot$ the metallicity, λ_{mm} the wavelength in mm, b a factor of the order of unity which depends on the grain environment, Ω the beam area in steradians and σ_{mm} the dust opacity at a wavelength of 1 mm associated with a column density of 1 H-atom cm^{-2}.

The dust thermal emission at FIR, submm and mm wavelengths has been studied in nearby molecular clouds as well as in external galaxies. Local cloud studies imply an index m between 1.5 and 2.5 for $\lambda > 200\mu$m, grain temperatures in the range 12 – 25 K, and values of $b\sigma_{\mathrm{mm}} Z/Z_\odot$ of the order of 10^{-26} H-atom cm^2 (see e.g. Hildebrand 1983; Pajot et al. 1986, 1989; Cox & Mezger 1989, Krügel & Chini 1994; Goldsmith et al. 1995). Draine & Lee (1984; hereafter DL) find $\sigma_{\mathrm{mm}} \simeq 7 \times 10^{-27}$ cm^2 per H-atom for diffuse gas.

Table 1. X-ray flux densities are in units of erg s^{-1} cm^{-2}. The 11″ scale flux densities were determined by scaling the IRAS data for the whole galaxy with the fraction of the CO(2–1) emission in the central beam. "tw" refers to this work, IS91 to Irwin & Seaquist (1991), IS92 to Irwin & Sofue (1992),Y89 to Young et al. (1989), H95 to Hawarden et al. (1995), E89 to Eales et al. (1989), RC3 to de Vaucouleurs et al. (1991), RSA to Sandage & Tammann (1981), R95 to Reichert et al. (1995), and S78 to Shostak (1978) where [a] and [b] refer to measurements made with the 300 ft and 82 ft telescopes respectively. All maps are centered on the radio coordinates.

NGC 3079 – Basic information

Other names:	PGC 29050	UGC 5387	4C 55.19
position	optical	radio	1.2 mm
RA(1950)	09 58 35.4	09 58 35.02	09 58 35.1
Dec(1950)	55 55 11	55 55 15.4	55 55 15.4
			ref.
Distance	15 Mpc		
Type	Scpec	SBS5	RSA, RC3
$D_{25} \times d_{25}$	$7.9' \times 1.4'$		RC3
$V_{\rm Hel}$	1145 km s^{-1}	1131 km s^{-1}	IS92, S78
pos. angle	165°		RC3
inclination	84°		IS91

	scale	value(s)	ref.
B_T^0	tot	10.45mag, 2.3 10^{10} L$_{\rm B\,\odot}$	RC3
X-ray	core	3.6 10^{-13}, 2.5 10^6 L$_\odot$	R95
X-ray	lobes	$\sim$ 2 10^{-14}, $\sim$ 1.4 10^5 L$_\odot$	R95
12 μm	tot	2.81 Jy	Y89
25 μm	tot	3.54 Jy	Y89
60 μm	tot	52.8 Jy	Y89
100 μm	tot	96.5 Jy	Y89
40 − 122 μm	tot	3.7 10^{10} L$_\odot$	Y89
350 μm	$\sim 80''$	10.0 ± 1.9 Jy	E89
450 μm	$\sim 80''$	2.1 ± 0.9 Jy	E89
800 μm	53″	920 ± 100 mJy	H95
1220 μm	tot	0.5 Jy	tw
25 μm	11″	1.5 Jy	
60 μm	11″	22.3 Jy	
100 μm	11″	40.8 Jy	
1220 μm	11″	31 mJy	tw
800 μm	16″	350 mJy	H95
CO(1–0)	21″	231 K km s^{-1}	tw
CO(2–1)	11″	306 K km s^{-1}	tw
HI	∼tot	94.8 Jy km s^{-1}, 5.0 10^9 M$_\odot$	S78[a]
HI	tot	109 Jy km s^{-1}, 5.8 10^9 M$_\odot$	S78[b]

The above formulae and constants, derived for local Galactic clouds, as well as semi-empirical dust grain models such as those of Mathis et al. (1977) and DL, have been used to convert the mm/submm thermal emission into gas column densities and masses for external galaxies ranging from normal spirals to Markarian galaxies (e.g. Chini et al. 1995) to IR ultra luminous and high redshift objects.

Detailed comparisons of the CO line ($I_{\rm CO}$) and thermal continuum mm (S_ν) emissions have recently been made in the central region of the Galaxy and in the Molecular ring, based on COBE mm/submm observations (Sodroski et al. 1994; 1995), as well as in half a dozen nearby galaxies, based on IRAM 30-m telescope data (Guélin et al. 1993, 1995, Sievers et al. 1994, Braine et al. 1995; Neininger et al. 1996; Dumke et al. 1997). The extragalactic studies, so far, dealt only with normal spirals and weak starburst galaxies, and showed a remarkably constant S_ν/I(CO) ratio in their central regions. In the periphery of the Sb spiral NGC 4565, where CO emission is almost undetectable, comparison of the 21-cm line emission with S_ν allowed the determination of the product $b\sigma Z/Z_\odot$, which was found to be very close to its local (DL) value for diffuse clouds (Neininger et al. 1996). Up to now, however, no detailed study has been made for the nuclear region of a truly active galaxy, with the exception of the modest starburst NGC 253 (Mauersberger et al. 1996). In this article, we report 11″ angular resolution observations of the λ1.2 mm CO line and dust continuum emissions in the bright starburst/AGN galaxy, NGC 3079.

Among the Milky Way's neighbours, the edge-on spiral NGC 3079 stands out for its unusual nuclear activity, illustrated by kpc radio lobes with a subarcsec radio core (de Bruyn 1977; Seaquist et al. 1978; Hummel et al. 1983; Duric & Seaquist 1988) and broad emission lines (Heckman et al. 1990; Filippenko & Sargent 1992). It is known to be one of the brightest sources of FIR continuum, CO line and H_2O maser emissions within 20 Mpc (its distance is $D \simeq 15$ Mpc, assuming a Hubble constant of 75 kms^{-1}Mpc^{-1}). NGC 3079 has recently been studied with high angular resolution in the 21-cm line (Irwin & Seaquist 1991; hereafter IS91) and in the CO (1–0) line (Irwin & Sofue 1992; Tacconi & Downes, in prep.). The CO shows a strong nuclear concentration and extended disk emission (Young et al. 1988). The HI data show a highly inclined disk (i = 84°, P.A. = 166°) with a scale-length of $\sim$ 10 kpc and height of 0.9 kpc (IS91); the peak HI column density is $N_{\rm HI} \approx 10^{22}$ H-atom cm^{-2} (assuming optically thin gas). The steeply rising rotation curve (which reaches at least 330 kms^{-1} in 0.4 kpc) reveals a large central mass.

2. Observations

All observations presented here come from the IRAM 30 meter telescope at Pico Veleta (Spain). The continuum observations were made using the 19-channel bolometer of the Max-Planck-Institut für Radioastronomie (Kreysa et al. 1993). The central frequency and bandwidth are 245 GHz and 70 GHz respectively (see Guélin et al. 1995 for details). Analysis of pointing scans on Mars and the quasar 0923+392 shows that the beamsize is about $\theta_{\rm fwhm} \approx 10.7''$. Calibration maps of Mars and Uranus during the bolometer observations (second half of March 1995) indicate that the conversion factor from observed counts to mJy is about 0.32 mJy count^{-1}. These values have been adopted throughout this work. We will refer to the 1.2 mm wavelength but all calculations have been made using the more precise value of 245 GHz.

Continuum maps were made by scanning in azimuth at a rate of 4 arcminutes per minute taking data every 2″ with a 1′ chopper throw. The end points of each scan were made to leave *at least* 100″ of blank sky to either side of the galaxy (roughly the radius of the array plus the chopper throw). Each azimuthal scan was shifted slightly in azimuth with respect to the preceding one

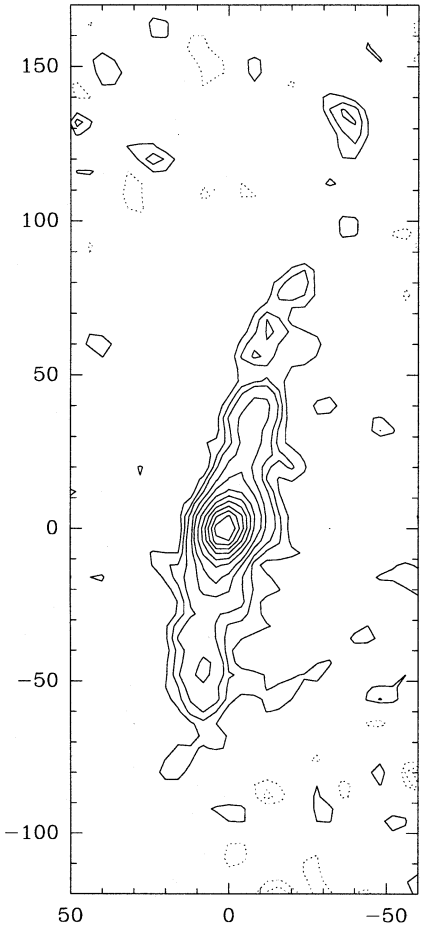

Fig. 1. Emission of NGC 3079 within a bandwidth of 70 GHz centered around 245 GHz. Offsets are in arcseconds with respect to the radio position given in Table 1. Contours are -8 -6 -4 4 6 8 12 16 22 28 34 40 46 52 mJy per 10.7″ beam. The noise level is 2 mJy beam^{-1} so the lowest contours are at 2σ. Negative contours are dashed.

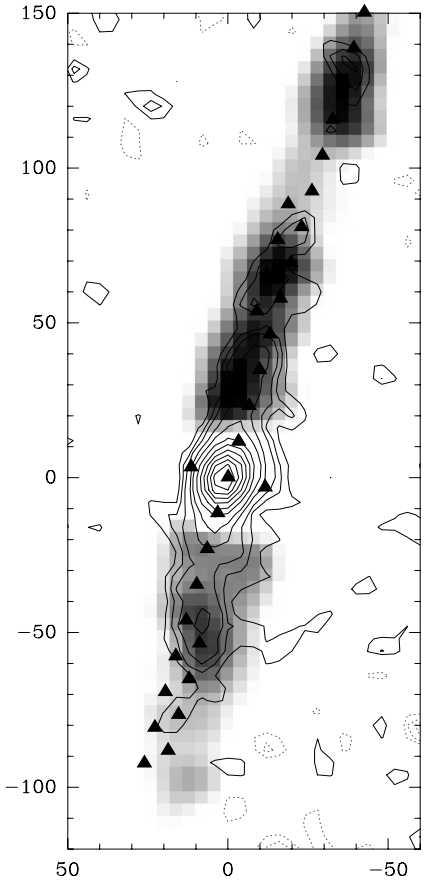

Fig. 2. Same as Fig. 1, superimposed on a grey scale HI map (IS91). Dark triangles mark the positions observed in CO. Note the good correspondance between the HI and 1.2 mm emission in the Northern maximum.

in order to match the orientation of the galaxy on the sky at the time of observation. The separation in elevation between scans was 4″. Individual maps were therefore parallelograms in Az-El space. The elevation coverage was determined by the change in orientation of the galaxy during the map. Typical maps were Az x El 270″ × 200″. The galaxy was observed in three parts – the central region and then a region centered on 3′ to the North and a southern region 2′ South (along the major axis).

^{12}CO was observed in the $1-0$ and $2-1$ transitions simultaneously with the 3mm and the two 1mm SIS receivers, two filterbanks of 512 × 1 MHz channels, and the autocorrelator. Pointing was checked every hour on the quasar 0923+392 and found to be accurate to $\lesssim$ 3″rms. System temperatures varied from 300 K to 400 K (T_a^* scale) at 110 and 115 GHz and from 500 K to 700 K at 220 and 230 GHz. Cold load calibrations were made every 4 or 8 minutes integration time depending on receiver and atmospheric stability. All molecular line observations were made from May 12 to 18, 1995. The beamsizes at the frequency of the ^{12}CO (2–1) and ^{12}CO (1–0) lines were measured (on Mars) to be $10.5'' \lesssim \theta_{230} \lesssim 11''$ and $\theta_{115} \approx 21''$.

As an independent pointing check, and to measure the central source size, the center and two points 12″ to either side along the minor axis were observed quickly after each pointing. In this way, errors along the minor axis are easily detected due to the difference in flux. Errors along the major axis are obvious from the central line profile. All maps are centered on the radio position given in Table 1.

3. Observational results

3.1. Bolometer observations

We show the full-resolution map of NGC 3079 at 1.2 mm in Fig. 1. The total spectral flux density is 0.5 Jy. The rms noise in the map is 2 mJy beam^{-1}. In Fig. 2 the same data are displayed with a grey-scale image of the HI emission (IS91) overlayed and triangles indicate the positions of the ^{12}CO observations. The secondary HI maximum 2′ North is detected. The bolometer and HI emission follow each other well out to HI column densities of about $N_{HI} \approx 5\ 10^{21}$ cm^{-2}. The HI peaks at $\sim 50''$ South and $\sim 70''$ North are apparent in the bolometer map as well. The noise level is reached at radii of about 100″ in the South and 150″ in the North.

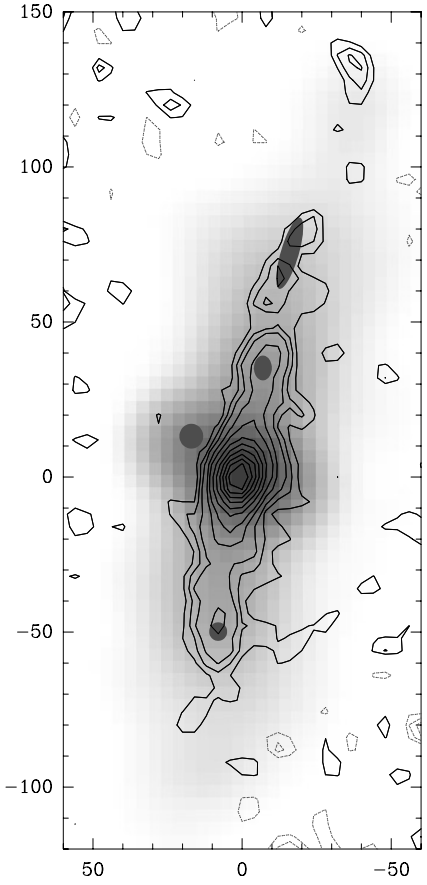

Fig. 3. Bolometer data as Fig. 2, grey scale is low-resolution radio continuum emission at 20cm obtained from N. Duric, and shaded ellipses mark the radio continuum maxima at 2.7 GHz from Seaquist et al. 1978. Note the good correspondance between the radio continuum and 1.2 mm maxima with the exception of the radio lobes.

In Fig. 3 we present the 1.2mm emission superimposed on a low-resolution grey scale map of the radio continuum at 20cm (Duric, priv. comm.). The shaded ellipses indicate radio continuum maxima from the higher resolution 2.7 GHz observations of Seaquist et al. (1978). Two aspects are apparent: the radio continuum and thermal dust maxima coincide well with the notable exception of the radio lobes (Duric & Seaquist 1988). The Northern maximum (at 130″ from the center) is also detected in the 20cm radio continuum maps presented by Condon (1983) and de Bruyn (1977) and can be seen in Hα at the edge of the map by Ford et al. (1986).

The central region of the 1.2 mm emission is shown at larger scale in Fig. 4 where the lowest contour marks the half-power level. The map is centered on the radio position at 20cm given by IS91 (their Table 3); the peaks coincide to better than 1″. Our bolometer observations were centered on the optical center (Table 1) but during reduction the map was shifted because the true center is clearly very close to the radio center.

At our resolution of 11″ at 1.2 mm the 30m telescope beam subtends about 0.8 kpc so we have no information on structures $\lesssim$ 300 pc. The distribution of the 1.2 mm emission perpendicular to the major axis is shown in Fig. 5. The half-power width of the central emission is $\lesssim 9''$ after deconvolving for the antenna beam. The other cuts shown in Fig. 5 show that the width is slightly greater away from the nucleus, typically $\approx 11 \pm 1''$. This can be explained by assuming that the central emission is the sum of a central source of radius $r \lesssim 100$ pc (1″) and an inclined disk. From Figs. 4, 5, and 6, it is readily apparent that the central emission is extended along the major axis. If one assumes a gaussian form, the corrected half-power width of the central source is $\approx 17''$ along the major axis. Two cuts are shown in Fig. 6 because the position angle (p.a.) of NGC 3079 changes from -13°in the inner disk to -17°at the Northern maximum. The peak of this feature is at 136″ from the nucleus.

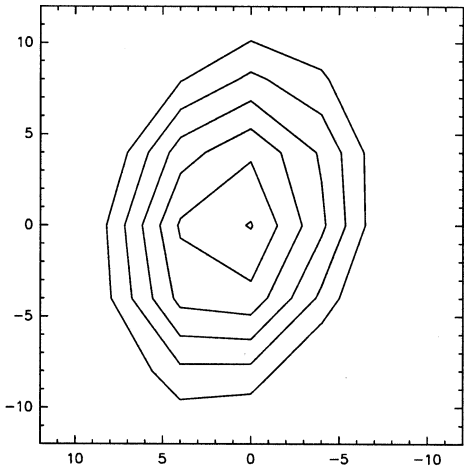

Fig. 4. The central kiloparsec of NGC 3079 at $\sim$ 1.2 mm. Offsets are in arcseconds with respect to the radio position given in Table 1. Contours are 30, 36, 42, 48, 54, 60 mJy per 10.7″ beam.

The emission detected by the bolometer is the sum of several types of emission: synchrotron, thermal free-free, molecular line (essentially ^{12}CO (2–1)), and, for the most part, thermal emission from dust. The breakdown of the weaker components will be discussed in Sect. 3.3; these components are then removed to leave only the thermal dust continuum.

3.2. Molecular line observations

Figs. 7a and 7b show the spectra along the optical major axis in the ^{12}CO (2–1) and ^{12}CO (1–0) lines. The ^{12}CO (1–0) and ^{12}CO (2–1) spectra show the same features. Spectra along the major axis are spaced by 12″, the two spectra either side of the nucleus are also 12″ from the center, and the remaining spectra are placed 6″ along the minor axis and 6″ along the major axis from the adjacent spectra (see Fig. 7).

A rare and striking feature is the extreme line width at the central position, $\Delta V_{\rm half-power} \approx 500\,{\rm km\,s^{-1}}$ and $\Delta V_{\rm zero-power} \gtrsim 650\,{\rm km\,s^{-1}}$ (Fig. 8), compared to the velocity range in the disk, $\Delta V_{\rm zero-power} \approx 500\,{\rm km\,s^{-1}}$.

The central ^{12}CO (1–0) and ^{12}CO (2–1) spectra are superimposed in Fig. 8. Despite the difference in angular resolution the shapes of the profiles are remarkably similar. This confirms

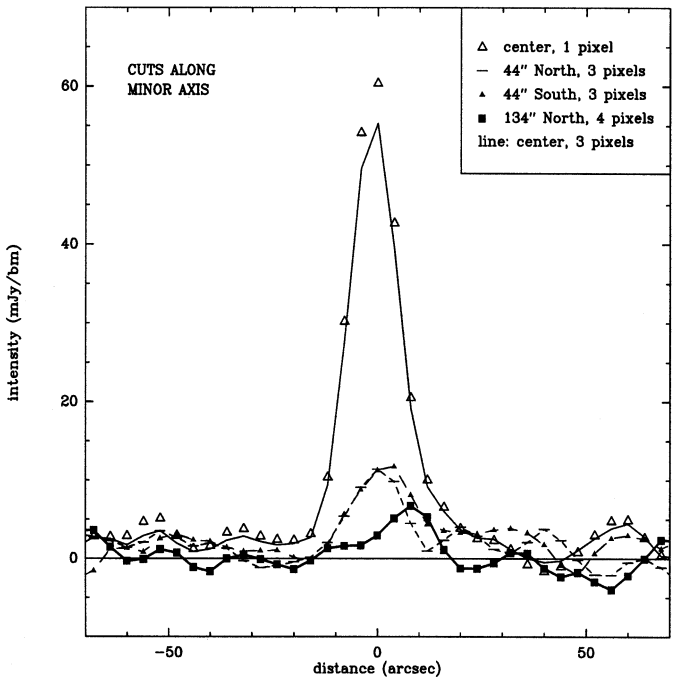

Fig. 5. Distribution of the $\sim$ 1.2 mm emission perpendicular to the major axis. 3 pixels 4″ each have been summed along the major axis except for the open triangles. Note the prominence of the central peak and that the half-power width near the nucleus is smaller than in the disk.

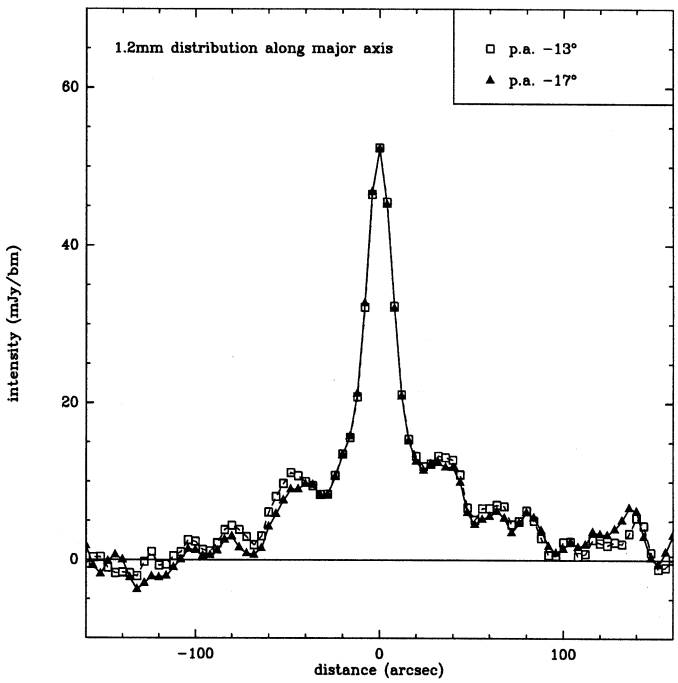

Fig. 6. Distribution of the $\sim$ 1.2 mm emission along the major axis. 3 pixels 4″ each have been summed along the minor axis. Filled triangles indicate a cut with a -17° position angle, showing the secondary maximum well, and open squares show the cut with a -13° position angle, more appropriate for the inner regions.

that the entire extent of the velocities is observed very close to the center and that the source is quite small.

The Northern maximum is detected in CO (Fig. 9) but is quite weak compared to what might be expected from the dust emission. As we shall see, this is because most of the 1.2 mm emission comes from dust associated with the atomic gas. This area corresponds to a region of massive star formation where the NII/Hα ratio is low, suggesting a low metallicity (Veilleux et al. 1995).

The radial distributions of the CO line intensities are displayed in Fig. 10. The nucleus stands out compared to the disk. Such an extreme nuclear concentration is typical of strongly interacting or perturbed systems.

The systemic (heliocentric) velocity from HI observations is $V_{\rm hel}$ = 1130 km s^{-1} (Shostak 1978; IS91). We find CO heliocentric velocities of $v_{\rm cen} \approx$ 1140 km s^{-1} from gaussian fits to the central spectra and $v_{\rm disk} \approx$ 1145 km s^{-1} from averaging the velocities at symmetrically opposite points in the disk, in agreement with Irwin & Sofue (1992).

The CO($\frac{2-1}{1-0}$) ratio is less than unity. From the central spectrum and the four surrounding positions observed 12″ from the center (cf. Fig. 7), we estimate CO($\frac{2-1}{1-0}$)$\sim$ 0.7. Assuming that the ^{12}CO (2–1) emission is distributed like the 1.2 mm emission yields a similar result.

3.3. Non-dust contributions to the observed flux

3.3.1. Molecular lines

The contribution of the ^{12}CO (2–1) line is

$$\frac{F_{\rm line}}{F_{\rm total}} \approx 0.054 \, \frac{I_{\rm CO(2-1)}}{S_{1.2}} \qquad (3)$$

where $S_{1.2}$ is in mJy and $I_{\rm CO(2-1)}$ is in K km s^{-1}) for our beamsize and a bolometer bandwidth of $\Delta\nu_{\rm bol}$ = 70 GHz.

The ^{13}CO (2–1) line strength is $\sim$ 0.1 of the ^{12}CO (2–1) line. All other line contributions are assumed to be negligible. Fig. 11 shows the fraction of the total emission due to the $J = 2 \rightarrow 1$ transition of ^{12}CO and ^{13}CO. It peaks at $\approx$35% at the center and decreases steadily with radius to less than 10%. About 25% of the total flux observed with the bolometer is due to the CO(2–1) lines alone.

3.3.2. Thermal free-free and non-thermal radiation

A good fit to the radio spectrum is obtained with a non-thermal spectral index of 0.72 and a thermal fraction of 10% at 10 GHz, where the data are from Seaquist et al. (1978), Israel & vander Hulst (1983), IS91, Condon (1987), Gioia & Gregorini (1980), and Niklas et al. (1995). Extending this to millimeter wavelengths, we estimate that 7% of the emission detected with the bolometer is due to thermal free-free and synchrotron radiation.

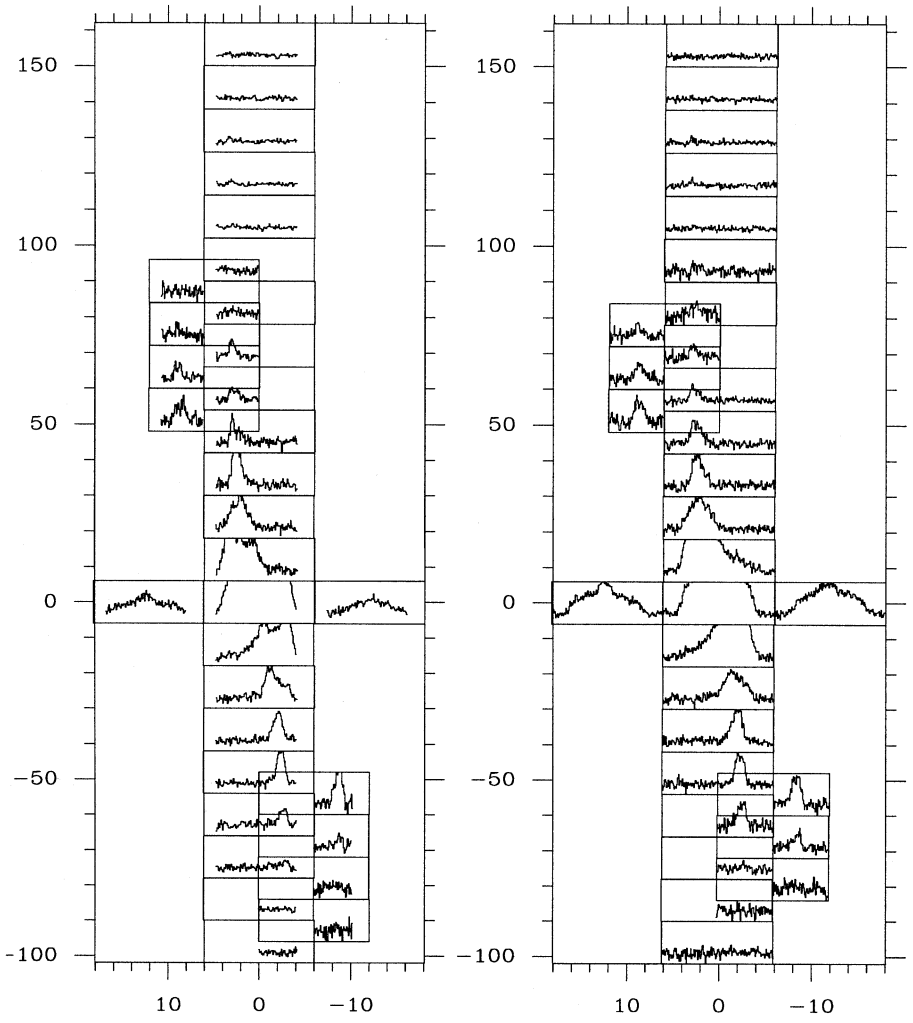

Fig. 7. ^{12}CO (2–1) emission of NGC 3079 at an angular resolution of $\approx$ 11″ (left) and ^{12}CO (1–0) emission of NGC 3079 at an angular resolution of 21″. Temperatures (y-axis of each spectrum) are in the main-beam scale and the range in each box is from −100 mK to 300 mK. The velocity (heliocentric) ranges from 700 to 1600 km s^{-1}. Offsets are in arcseconds along the major and minor axes (position angle -15°).

4. Properties of the dust and gas

Once the contributions to the 245 GHz continuum from sources other than thermal dust emission have been estimated and removed, we can try to determine the emissivities of the dust in the atomic and molecular gas components. First, we derive approximate temperatures for the cool component of the dust. We find that no cold (*i.e.* $T_d \lesssim 20$ K) dust is necessary to account for the emission from the nucleus. However, the data for the disk show that, contrary to the claims of Eales et al. (1989), a cold component is necessary to account for the disk emission. This illustrates the importance of high angular resolution to be able to separate the central and extended components in a galaxy.

4.1. Dust temperature

The nucleus and disk being very different at many wavelengths, we try to separate the center and disk to determine dust temperatures.

4.1.1. Dust emissivity

Throughout the analysis, two different grey-body curves are used to fit the data. It is frequently assumed, for observational and theoretical reasons (DL; Chini et al. 1995; Krügel & Siebenmorgen 1994; Hildebrand 1983), that the emissivity at long wavelengths varies as ν^2. We are only concerned with wavelengths $\lambda \gtrsim 60\,\mu$m so, in order to provide a continuous emissivity law, we use

$$\epsilon_\nu = 1 - \exp(-\nu^2/\nu_t^2) \quad (4)$$

where ν_t is the frequency at which the dust emission starts becoming optically thick, taken here to be $\nu_t = c/40\,\mu$m, but we also use the discontinuous law taken from Hildebrand (1983):

$$\begin{aligned} \epsilon_\nu &\propto \nu^2 \quad (\text{for } \nu < 1200\,\text{GHz}, \lambda > 250\,\mu\text{m}) \\ &\propto \nu \quad (\text{for } \nu > 1200\,\text{GHz}, \lambda < 250\,\mu\text{m}). \end{aligned} \quad (5)$$

4.1.2. Central region

IRAS measurements

In order to separate the nucleus and disk at wavelengths such as 100 μm, we need higher resolution observations of emission

with a similar distribution. One of the best correlations in all of astrophysics is between the radio continuum (essentially non-thermal synchrotron radiation) and the FIR emission traced by IRAS (e.g. Dickey & Salpeter 1984; Condon et al. 1991). The relationship is also very close within galaxies where the radio and FIR emission are correlated on sub-kpc scales (Beck & Golla 1988; Boulanger & Pérault 1988; Bicay et al. 1989). The FIR-to-radio ratio decreases slightly with radius, showing that the FIR emission is more centrally concentrated (Bicay & Helou 1990; Rice et al. 1990). Using the radio data to scale the FIR emission is thus expected to result in a slight underestimate of the central FIR flux. Seaquist et al. (1978) observed NGC 3079 at 2.7 GHz with 9″ resolution and found that 34% of the total flux was in the central beam. They obtained a similar fraction at 8.1 GHz in a smaller beam. About 40% (39 Jy at 100 μm) would be a reasonable guess for an 11″ beam. Very similar values are obtained from de Bruyn's (1977) measurements.

A similar correlation exists between CO and FIR emission, albeit with greater scatter (e.g. Young et al. 1989). If we use the 11″ resolution CO(2–1) observations to scale the FIR emission, we obtain 40 Jy at 100 μm.

Based upon the above, we take the central 100 μm flux density to be 40 Jy and assume the same fraction for the central 60 μm point shown in Fig. 13.

Submm measurements

Scaling the submillimeter measurements is more difficult because no whole galaxy fluxes are available. The Eales et al. (1989) measurements of the 350 μm and 450 μm fluxes were made with 86″ and 81″ beams respectively and a further (smaller) amount of flux may have been lost by chopping into the galaxy. Hawarden et al. (1995) observed NGC 3079 at 800 μm with a 16″ beam and covered a roughly 53″ region. For the central flux densities, we regard the Eales et al. values as upper limits due to the large beam size. The distribution of the 800 μm emission is probably quite similar to that of the 1.2 mm so we have scaled their data to 11″ by assuming that the 800 μm emission follows our map.

Central dust temperature

The resulting spectrum for the central 11″ is shown in Fig. 12 (filled squares and lower curves) with two *single temperature* curves which fit the observed data quite well. Our preferred curve, shown as a solid line, is a 32 K blackbody modified by the first emissivity law above. The dashed line is a 37 K blackbody with the second emissivity law above. We adopt $T_{\rm dust,center}$ = 32 K.

As discussed above, using the radio observations to scale the FIR emission is likely to lead to a slight *underestimate* of the 100 μm flux density. If the IRAS dust color temperature decreases with radius, the 60 μm and 25 μm central flux densities will be underestimated by a slightly larger factor.

No cool or cold dust is necessary to fit the central spectrum.

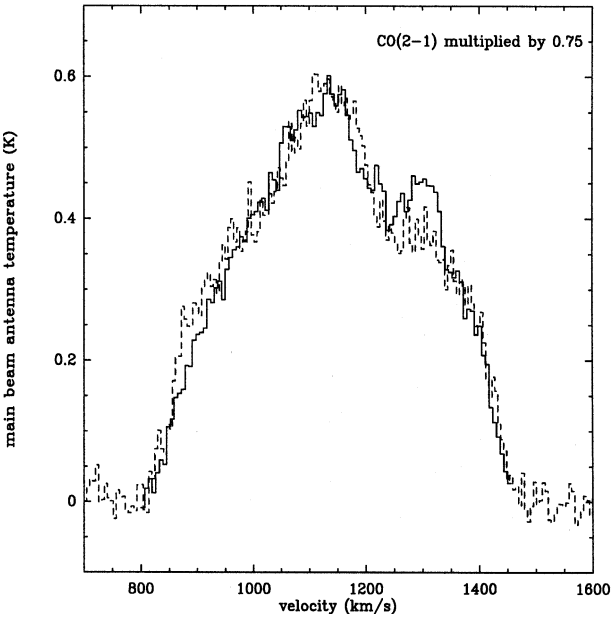

Fig. 8. Central ^{12}CO (1–0) (dashed line) and ^{12}CO (2–1) (solid line) spectra at 21″ and 11″ resolution respectively. To make comparison easier, the ^{12}CO (2–1) spectrum has been multiplied by 0.75.

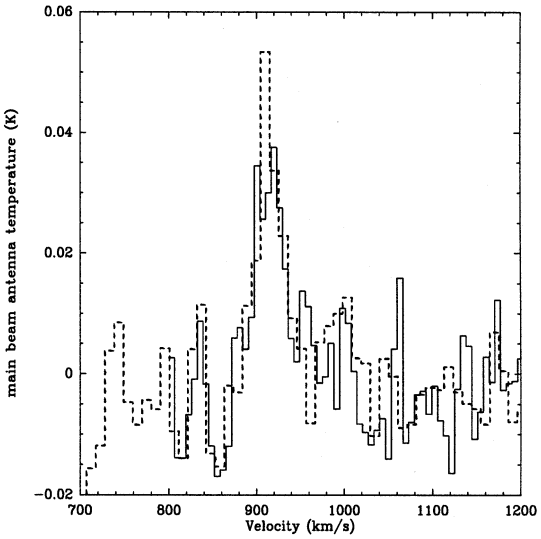

Fig. 9. ^{12}CO (1–0) (dashed line) and ^{12}CO (2–1) (solid line) spectra of the secondary maximum. Two positions at radii of 120″ and 132″ have been summed to increase the signal-to-noise ratio. No attempt has been made to correct for the different angular resolutions.

4.1.3. Disk of NGC 3079

The "disk" emission is defined here to be the total minus the central flux and these values are plotted as open symbols in Fig. 12. The "total" emission for the submm points was estimated using the published beamsizes and assuming that the distribution was that of the 1.2 mm emission. Although the temperature dependence of the emission at 350 μm and 450 μm is much stronger than at 1.2 mm, the situation is not like at 100 μm where the cold dust is simply not detected.

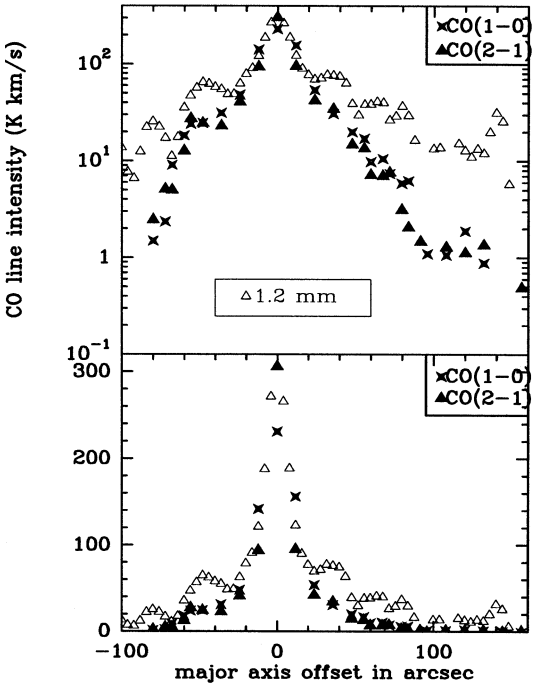

Fig. 10. Major-axis distribution of the ^{12}CO (1–0) (stars) and ^{12}CO (2–1) (triangles) integrated emission. For comparison, the 1.2mm emission has been scaled to the ^{12}CO (2–1) maximum and is represented by open triangles. Upper plot is with log scale and lower with linear scale. North (low-velocity) is positive offset. The angular resolution of the 1.2 mm and ^{12}CO (2–1) observations is 11″ while the ^{12}CO (1–0) beamsize is 21″.

We therefore mark the 350 μm point as an upper limit. The 450 μm point is likely to be underestimated because it appears incompatible with the 350 μm and 800 μm values. The solid line through the open squares in Fig. 12 is a two-temperature curve with dust temperatures of 15 K and 34 K. No single temperature can fit the 1.2 mm to 60 μm data for the disk, in contrast with the central region.

A second two-temperature curve is shown as a dashed line using the discontinuous emissivity law but is not as good a fit. For the calculations involving a dust temperature for the disk, we adopt 17 K.

4.1.4. How certain can we be?

Many of the properties of dust grains are still poorly known. In particular, it has been suggested that the emissivity may vary as ν^m where $m \approx 1.5$ at long wavelengths rather than $m = 2$ as we have assumed in both emissivity laws. This is more important than the precise value of the cross-section σ because it affects the shape of the spectrum.

A not implausible fit to the whole-galaxy fluxes from 1.2 mm to 100 μm can be obtained by fitting a $\lambda^{-1.5}$ law with a single dust temperature. This is wrong and illustrates the sort of error that can be made without enough resolution to isolate the major components (disk and nucleus, in spiral galaxies).

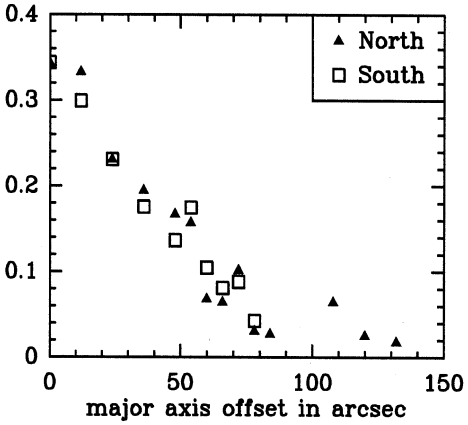

Fig. 11. Contribution of the CO(2–1) lines to the observed bolometer flux along the major axis.

As neither central nor "disk" data are available at intermediate wavelengths, we fit the 1.2 mm and 100 μm points in Fig. 12 for the center and disk. For the disk, the flux at 60 μm is significantly below what is "expected" from a $m = 1.5$ fit. For the center, the flux at 60 μm is significantly *above* what is expected from the fit. The former is not a problem because some fraction of the 60 μm emission comes from warmer dust detected at 25 μm. In the center, however, a dust temperature of ~ 50 K is required to fit the 100 μm and 1.2 mm points and this yields much more flux at 60 μm than observed. A multi-temperature fit is not constrained.

A possibility that we cannot exclude is that the grains are different in the central region and disk. By fitting the disk data with a $\nu^{1.5}$ emissivity law, it is possible to substantially raise the temperature of the "cool" dust component. Note that if the dust temperatures were higher than what we derived above, the $N(\mathrm{H_2})/I_{\mathrm{CO}}$ factor should be reduced further.

4.2. The dust cross-section σ in the disk atomic gas

The column density of the atomic gas is well determined from the 21cm line observations. The same cannot be said for the H_2 column density. It is thus logical to try to determine the dust cross-section σ in the atomic gas first.

The most direct method is simply to apply Eq. (1) where only atomic gas is detected so that the cross-section is measured to within the uncertainty in $B(\nu, T_d)$. In this way, Neininger et al. (1996) found $\sigma_{1.22\,\mathrm{mm,HI}} = 5 \times 10^{-27}\mathrm{cm}^2$, very close to the DL value.

Although CO is detected in the Northern maximum, the column density of H_2 is an order of magnitude lower than that of HI. We then obtain $\sigma_{1.22\,\mathrm{mm,HI}} \lesssim 7 \times 10^{-27}\mathrm{cm}^2$. Given the likely $N_{\mathrm{H_2}}$ column density, it would be reasonable to reduce this by $\sim$10%. If the dust temperature were 20 K (15 K), then $\sigma_{1.22\,\mathrm{mm,HI}} \approx 5 \times 10^{-27}\mathrm{cm}^2$ ($8 \times 10^{-27}\mathrm{cm}^2$). The beam used for the HI observations (15″ × 17″ from IS91) is larger than for the CO and 1.2 mm continuum. If the thickness of the HI disk or the size of the maximum results in beam dilution, or if

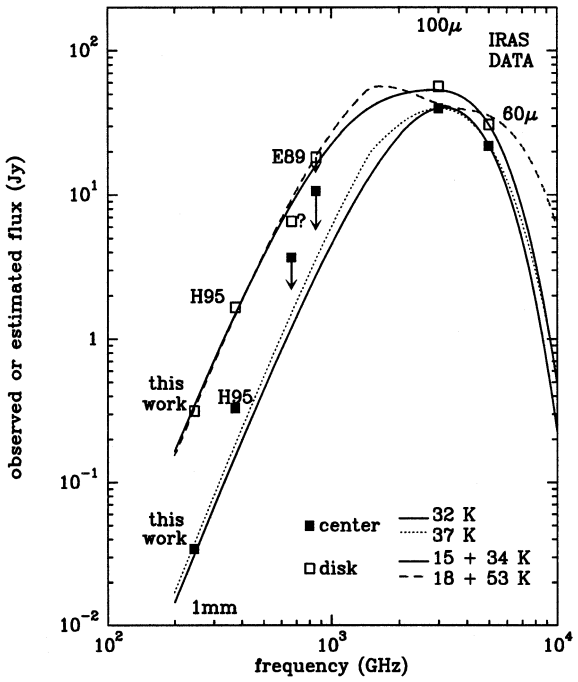

Fig. 12. Decomposition into central (filled squares) and disk components (open squares). The 1.2 mm points come directly from our observations. The other points represent extrapolations from either partial (E89, H95) or total (IRAS) coverage at poorer angular resolution. See Sect. 4.1 for details. The curves represent single temperature approximations to the "central" data and two-temperature fits to the "disk" data. Two lines are present for each; the solid line is with the continuous emissivity and the dotted or dashed line is with the discontinuous emissivity law (Sect. 4.1).

the HI is partially optically thick, then our values are somewhat overestimated.

A second way of determining the cross-section of the dust in atomic gas clouds which does not restrict the dataset to points with negligible CO emission consists of fitting all the data to Eq. (1), which then becomes

$$\frac{S_\nu}{\Omega} = N_{\rm HI}\,\sigma_{\nu,\rm HI}\,B_{\nu,T_{\rm d},\rm HI} + 2\frac{N(\rm H_2)}{I_{\rm CO}}\,I_{\rm CO}\,\sigma_{\nu,\rm H_2}\,B_{\nu,T_{\rm d},\rm H_2}.$$

We treat $N_{\rm HI}$ as an observable because of the small error in going from $S_{\rm HI}$ to $N_{\rm HI}$, even if the HI is partially optically thick. $I_{\rm CO}\ 2N(\rm H_2)/I_{\rm CO}$ is simply $2N_{\rm H_2}$, the column density of H-atoms in molecular hydrogen. Braine et al. (1995) obtained $\sigma_{1.22\,\rm mm,HI} = 5.6\pm2\times10^{-27}\rm cm^2$ in this way for the spiral galaxy NGC 4631. In NGC 3079, the points at 0 and $\pm12''$ were not included because the HI is detected in absorption. We now obtain $\sigma_{1.22\,\rm mm,HI} = 5.3\times10^{-27}\rm cm^2$ for $T_{\rm dust} = 17\,\rm K$, in agreement with the previous determinations. We adopt this cross-section as our reference value.

4.3. $N(\rm H_2)/I_{\rm CO}$ in the disk

Assuming $\sigma_{\rm H_2} = \sigma_{\rm HI}\,b\,Z/Z_\odot$, where $b = 1$ and $Z = Z_\odot$ is assumed for the dust in atomic gas clouds, we can estimate the mass of molecular gas in the disk of NGC 3079.

Table 2. Dust cross-sections

reference	$\sigma/\sigma_{\rm DL}$	medium
Krügel & Chini (1994)	1.7	general, galaxies
Pajot et al. 1986	1.2	
Pajot et al. 1989	1.8	towards Gal. cen.
Pollack et al 1994	1.7	mol clouds, acc. disks
Goldsmith et al. 1995	1.2	GMC

From the fit described above, we obtain the product $N(\rm H_2)/I_{\rm CO(2-1)}\,\sigma_{\nu,\rm H_2}$. We can turn this into a relationship between bZ and $N(\rm H_2)/I_{\rm CO(2-1)}$. We find

$$\sigma_{\rm H_2} = \sigma_{\rm HI}\,(\frac{N(\rm H_2)/I_{\rm CO(2-1)}}{1.8\,10^{20}})^{-1}\,\rm cm^2H^{-1}\quad or$$
$$N(\rm H_2)/I_{\rm CO(2-1)} \approx \frac{1.8\times10^{20}}{b\,Z/Z_\odot}\,\rm cm^{-2}(K\,km\,s^{-1})^{-1} \qquad (6)$$

Let us assume that $Z \approx Z_\odot$ for the disk of NGC 3079. Several theoretical and observational estimates exist for bZ or $\sigma_{1.22,\rm H_2}$. Expressed as a cross-section per H-atom and normalized to the DL value, we give several recent values for σ in Table 2. Only long-wavelength determinations are included in order to minimise the importance of the emissivity power-law index m (cf. Eq. 1). bZ is thus likely to be between 1 and 2, leading to a conversion ratio of $N(\rm H_2)/I_{\rm CO(2-1)} = 1-2\times10^{20}\,\rm cm^{-2}(K\,km\,s^{-1})^{-1}$. This value is slightly lower than has frequently been used for the Galaxy (Solomon et al. 1987; Strong et al. 1988) but within the range of "standard" values (Dickman et al. 1986; Richardson & Wolfendale 1988; Bloemen et al. 1990).

For $b_{\rm mol}Z = 1.5$ (Table 2), the mass of gas in the molecular medium is $\sim 2.2\,10^9\,\rm M_\odot$ (including He).

The CO($\frac{2-1}{1-0}$) intensity ratio is ~ 0.7, typical both of galactic disks and of ultraluminous galaxies (Radford et al. 1991; Casoli et al. 1988). This means that $X = N(\rm H_2)/I_{\rm CO(1-0)} \sim 0.7\,N(\rm H_2)/I_{\rm CO(2-1)}$ or $X \approx 10^{20}\,\rm cm^{-2}(K\,km\,s^{-1})^{-1}$..

4.4. $N_{\rm H_2}$ in the center

In the central region, the conversion must be lower. This is already apparent from the extreme line-to-continuum ratio. Nearly *half* of the flux measured with the bolometer comes from the CO(2–1) lines!

The strong central peak of the CO emission implies that we are observing emission from the center and not foreground/background gas. In contrast, the HI emission is very spread out so we adopt a column density of $N_{\rm HI} = 10^{22}\,\rm cm^{-2}$ along the line of sight towards the center. $N_{\rm HI}$ may in fact be somewhat higher, in which case the $N(\rm H_2)/I_{\rm CO}$ factor derived for the center would be lower.

In the following, we subtract the 1.2 mm due to the HI component from the total dust emission in order to obtain the 1.2 mm emission due to dust in the molecular gas. $S_{\rm H2} = S - N_{\rm HI}\sigma_{\rm HI}B_{1.2\,\rm mm,17\,K}$. We then use this to estimate the $\rm H_2$

column density in the central 11″

$$N_{\rm H_2} = \frac{S_{\rm H2}}{2bZ\Omega\sigma_{\rm HI}B_{1.2\,{\rm mm},32\,{\rm K}}}$$

which can be equated with the standard formula

$$N_{\rm H_2} = I_{\rm CO}\, N({\rm H_2})/I_{\rm CO}.$$

This yields a relationship between bZ and $N(\rm H_2)/I_{\rm CO}$.

4.4.1. Estimating bZ

The parameter b reflects the grain properties with respect to the diffuse gas. Fluffy agglomerates have a high b; bare cores have a low b (e.g. Ossenkopf & Henning 1994). The nucleus of NGC 3079 is clearly not quiescent and the dust temperature is significantly higher than in a standard galactic disk. The net effect on b is thus difficult to assess. In an effort to be conservative, we assume $b = 1$ for the moment and come back to the question later. We note that Guélin et al. (1993; 1995) and Mauersberger et al. (1996) explicitly took $b = 1.9$ in their studies.

The metallicity Z is known to be higher in galactic nuclei than in galactic disks. Guélin et al. (1995) and Mauersberger et al. (1996) used $Z = 3Z_\odot$. We adopt a metallicity of $2\,Z_\odot$, however, because (a) the CO emission in NGC 3079 is very centrally concentrated, so it is not unlikely that disk gas has recently fallen into the center and (b) there is now evidence that the average metallicity at the solar circle may in fact be closer to $0.7\,Z_\odot$ (Sofia et al. 1994; Cardelli et al. 1996; Mathis 1996). $2\,Z_\odot$ is thus a *conservative* estimate of the metallicity in the center of NGC 3079.

For $b = 1$ and $Z = 2Z_\odot$, the mass of gas in the molecular medium in the center of NGC 3079 is $\sim 1.5\,10^8\,{\rm M}_\odot$ (including He).

4.4.2. The $N(\rm H_2)/I_{\rm CO(2-1)}$ ratio

Setting $\sigma_{\rm H_2,center} = b\,Z\,\sigma_{\rm HI}$ with $bZ = 2$, we find

$$N({\rm H_2})/I_{\rm CO(2-1)} \approx 3\times10^{19}\,{\rm cm^{-2}(K\,km\,s^{-1})^{-1}} \quad \text{or} \qquad (7)$$

$$N({\rm H_2})/I_{\rm CO(1-0)} \approx 2\times10^{19}\,{\rm cm^{-2}(K\,km\,s^{-1})^{-1}} \qquad (8)$$

This is substantially below most estimates although reserves have frequently been expressed about whether "standard" values can be applied to galactic nuclei.

4.4.3. Possible errors

Our estimate of $N(\rm H_2)/I_{\rm CO}$ for the center of NGC 3079 is an order of magnitude below "standard" values so it is worth looking at how robust this value is.

1) We have adopted a conservative (low) value of Z. If Z were higher, we would obtain an even lower value for $N(\rm H_2)/I_{\rm CO}$.

2) We have adopted a low dust temperature. If the *dust temperature* were higher, such as the 37 K of our second fit, then again we would obtain an even lower value for $N(\rm H_2)/I_{\rm CO}$.

3) We have adopted a conservative value of b. If b were significantly below unity, this would suggest partial grain destruction. In fact, even $b = 1$ suggests that the mantles expected to form efficiently in dense gas (Walmsley 1991) have either not formed or have already been evaporated to their diffuse gas levels. This is discussed further in Sect. 5.3 where we conclude that b is not $\ll 1$.

While the CO emission is subject to both rms and systematic errors, the CO(1–0) value is in agreement with those obtained several years earlier by Braine et al. (1993) and Young et al. (1986). We estimate a CO($\frac{2-1}{1-0}$) ~ 0.7 (Sect. 3.2), already fairly low for a galactic nucleus (Braine et al. 1993). If our ^{12}CO (2–1) intensity were an underestimate, then again one would obtain an even lower value for $N(\rm H_2)/I_{\rm CO}$.

The contribution of the HI column density is quite small towards the center. Even if we ignore it entirely, the $N(\rm H_2)/I_{\rm CO}$ factor only increases by 10%.

The 1.2 mm flux could be underestimated. While an error of $\lesssim 20\%$ cannot be excluded, a higher error seems unlikely. Our measured total flux is equal to that of Chini et al. (1986) and far above the extrapolation of Eales et al. (1989). Many maps were made over several days and several maps of planets have been used to estimate the conversion factor from counts to mJy beam^{-1}. The rms errors near the center are negligible and there is absolutely no risk of chopping into the galaxy. In order to estimate the contribution of spectral lines, we used the recent estimate of 70 GHz for the bandwidth. Were the bandwidth narrower, the value for the central $N(\rm H_2)/I_{\rm CO}$ ratio determined here would be lower.

Could a substantial mass of cool dust be present in the center? If we assume that the cool dust in the center is not cooler than the 17 K we take for the disk, then the amount of cool dust that could be present is $M_{\rm cool\ dust} \lesssim 0.1-0.5 M_{32\,{\rm K\ dust}}$ (depending on the errors assumed and emissivity law used). This is not enough to affect our conclusions. Evidence for cool dust near the much more quiescent center of the Milky Way is weak (e.g. Sodroski et al. 1995).

We conclude that the $N(\rm H_2)/I_{\rm CO}$ factor in the center of NGC 3079 is at least a factor of several and probably a full order of magnitude below the most frequently used values.

5. The central $N(\rm H_2)/I_{\rm CO}$ ratio

5.1. CO line $N(\rm H_2)/I_{\rm CO}$ calculations

The $N(\rm H_2)/I_{\rm CO(2-1)}$ factor for optically thin CO is $0.5 - 1\ 10^{19}\,{\rm cm^{-2}(K\,km\,s^{-1})^{-1}}$, depending on how close the excitation is to LTE (Wild et al. 1992; Mauersberger et al. 1996; CO abundance of 10^{-4}). Our ^{13}CO measurements show that $^{12/13}$CO(2–1) $\approx$ 8. Assuming an intrinsic abundance ratio of 30, the optical depth in the ^{12}CO (2–1) line is about 4, leading to $N(\rm H_2)/I_{\rm CO(2-1)} \approx 2 - 4\,10^{19}\,{\rm cm^{-2}(K\,km\,s^{-1})^{-1}}$. The optical depth is unlikely to be overestimated because the low CO($\frac{2-1}{1-0}$) ratio (~ 0.7) implies that $\tau_{^{12}\rm CO} \geq 1$ and the CO(2–1) line has a higher optical depth. Assuming that the ^{13}CO (2–

1) is optically thin and in LTE leads to $N(H_2)/I_{CO(2-1)} \approx 4\,10^{19}\,cm^{-2}(K\,km\,s^{-1})^{-1}$, or somewhat less if not in LTE.

These values are in good agreement with the dust-based $N(H_2)/I_{CO}$ conversion factors and suggest that a dust parameter b significantly greater than unity is unlikely in this situation.

5.2. Importance for ultraluminous IRAS galaxies

While NGC 3079 is clearly not an ultraluminous IRAS galaxy, its nucleus appears "active" in ways similar to what is observed in the very luminous objects. The proximity of NGC 3079 makes it useful as a "stepping stone" towards the very luminous systems with the advantage that it can be studied in more detail and with higher signal-to-noise data.

The CO luminosity in some ultraluminous IRAS galaxies is so great that using a "standard" $N(H_2)/I_{CO}$ factor yields gas masses of order or perhaps greater than the dynamical mass of the system (Shier et al. 1994; Solomon et al. 1997). We will take Arp 220 as an example. The CO(2–1) luminosity of the core is about $2.5\,10^9$ K km s^{-1} pc^2 (Radford et al. 1991; Scoville et al. 1991). Scoville et al. (1991) estimate that the nuclear ($r < 1''$) H_2 mass is $1.8\,10^{10}\,M_\odot$, similar to the dynamical mass. Using the factor we derive for the center of NGC 3079, we obtain $M_{H_2} \sim 1.6\,10^9\,M_\odot$ for the core of Arp 220 including the He associated with the H_2 ($H_0 = 75$ km s^{-1} Mpc^{-1} for all).

If we reduce the $N(H_2)/I_{CO}$ factor by another factor 2.5 (resulting from the higher $bZ\sigma$ values used by e.g. Mauersberger et al. 1996 and Guélin et al. 1995), then the gas consumption time in Arp 220 becomes an uncomfortably short $\tau_{burst} \sim 5$ Myr.

A typical full-sized spiral galaxy has a few $10^9\,M_\odot$ of gas. Thus, if Arp 220 (or other ultraluminous galaxies) is the result of the merger of two large spirals, most of the ISM is still outside the core.

5.3. Is there destruction of grain mantles?

We have been quite conservative in our treatment of the 1.2 mm data. As mentioned in Sect. 4.4.1, however, we know very little about the b value in such a complex non-quiescent nucleus. It is worth stressing that this is one of the new aspects of the observations presented here. A higher gas mass (and thus $N(H_2)/I_{CO}$) means that b must be lower, implying partial destruction of the grains. By taking $b = 1$ earlier, we already supposed that the grains were similar to those in the diffuse gas, *i.e.* that they had not developed thick mantles or become fluffy as might be expected in a cool dense medium (Léger et al. 1985, Rengarajan 1984; Krügel & Chini 1994; Ossenkopf & Henning 1994). It should be noted that partial grain destruction, and mantle evaporation in particular, has the double effect of reducing the thermal dust emission and increasing the gas phase abundances of C and O.

Our observations and the preceding discussion show that $b \gg 1$, such as in a cool dense medium, is not appropriate for the center of NGC 3079. Among nearby galaxies, NGC 3079 is an excellent candidate for partial grain destruction due to the extreme line widths observed near the center (e.g. Heckman et al. 1990; Filippenko & Sargent 1992) and the strong H_2 1 − 0 S(1) line emission (Hawarden et al. 1995). The Hα emission from the nucleus is, however, heavily absorbed (Veilleux et al. 1995). Furthermore, our estimate of the column density from ^{13}CO measurements is in agreement with that calculated from the 1.2 mm dust emission using $b = 1$. $b \ll 1$ appears incompatible with the observations.

In the centers of ultraluminous galaxies, the situation may be expected to be more extreme than in NGC 3079. Near-IR observations show that the extinctions determined towards the nuclei of starburst galaxies are huge (e.g. Sturm et al. 1996) so the column density of dust must be very high. Furthermore, there is evidence that the dust emission may be optically thick for $\lambda \lesssim 100\,\mu$m in ultraluminous IR galaxies (Downes et al. 1993). Again, $b \ll 1$ appears in contradiction with the observations.

A 50% destruction of grains ($b = 0.5$) by shocks cannot be excluded by the arguments above but would only raise the gas masses (and $N(H_2)/I_{CO}$) by a factor 2. This would leave our conclusion essentially unchanged but would imply a profound modification of the physics and chemistry with respect to no grain or mantle destruction.

5.4. The interstellar medium of NGC 3079

Perhaps the first consequence of our measurements is that the atomic gas dominates the ISM of NGC 3079. Only in the center, and only by a small margin, is the column density of molecular hydrogen greater than that of atomic hydrogen. Precise values for N_{HI} towards the center are not known due to the absorption. The mass of molecular gas is far below the dynamical mass of the galaxy at all scales accessible to these observations (*i.e.* scales $\gtrsim 500$ pc).

5.5. NGC 3079: "Active" or "Normal"?

In their study of the mm continuum emission of a wide variety of galaxies, Chini et al. (1995) identified two apparently distinct groups, which they termed "active" and "normal". The active galaxies, Markarians, do not appear to have a cool dust component and as a result, the ratio of IR luminosity to gas mass is high, $L_{IR}/M_{gas} \approx 90$. The normal sample contains a cool component and has $L_{IR}/M_{gas} \approx 6$. Their observations were global, observing more distant galaxies with a larger beam.

The advantage of observing a closer system such as NGC 3079 with a smaller beam is clear from our observations. The center of NGC 3079 appears not to contain cool dust and has $L_{IR}/M_{gas} \approx 100$ while the disk contains a component with $T_d < 20$ K, has $L_{IR}/M_{gas} = 6 - 7$, and seems normal in all other respects as well. From our observations, the center of NGC 3079 indeed appears as a local scaled-down version of the IR ultraluminous galaxies. The lack of cool dust suggests that gas masses can be estimated from IRAS observations. Most importantly, here we have a local example of a galaxy in which stars are forming very efficiently in a region (the center) where the gas mass is only $1.5\,10^8\,M_\odot$.

6. Conclusions

From the 1.2 mm, CO(2–1), and CO(1–0) maps of NGC 3079 presented here combined with previously published data, we obtain the following results for NGC 3079:

(a) Most of the central flux at 1.2 mm and in the CO lines is not due to a point-like source. The thermal dust emission follows the CO, HI, and non-thermal radio emission quite closely except for the radio lobes.

(b) The mass of molecular gas derived from the thermal dust emission is an order of magnitude lower than that derived from "standard" Galactic disk $N(\mathrm{H_2})/I_{\mathrm{CO}}$ ratios.

(c) No evidence is found for large quantities of cool dust in the central $11''$. A 32 K dust spectrum fits the data to wavelengths to 60 μm.

(d) In the disk, the long wavelength thermal dust emission is dominated by a cool component ($T_{\mathrm{dust}} \sim 15 - 20\,\mathrm{K}$).

(e) The I_{CO} to $N_{\mathrm{H_2}}$ conversion factor in the disk appears typical of galactic disks, including our own.

(f) We show that if we were not able to separate the central and disk components of the 1.2 mm emission, our image of NGC 3079 would be very different, and probably wrong.

Our picture of the central region, derived in Sects. 4 and 5, is one where most of the dust is at $T \sim 32\,\mathrm{K}$. The gas mass in the central $11''$ is of order $1.5\,10^8\,\mathrm{M}_\odot$ and the optical depths in the ^{12}CO (1–0) and ^{12}CO (2–1) lines are $\tau \gtrsim 1.3$ and $\tau \gtrsim 4$ respectively.

Most of the gas is probably at temperatures $T_{\mathrm{ex}} \sim 30\,\mathrm{K}$ which results in a larger contribution of the ^{12}CO (2–1) line in the bolometer band than for more quiescent galaxies.

Concerning the emission properties of dust, we confirm the values for the cross-section of dust associated with atomic gas found in other galaxies (Neininger et al. 1996; Braine et al. 1995; Dumke et al. 1997). The agreement with the calculations by Draine & Lee (1984) is excellent. In the center of NGC 3079, we conclude that the emission properties of dust ($'b'$ parameter) are not enhanced with respect to the atomic medium. The central dust emission may in fact be reduced slightly due to evaporation of the dust grain mantles, resulting in increased CO emission.

Acknowledgements. We wish to thank Robert Zylka of the MPIfR for helpful suggestions and the use of his software for the continuum observations. We also wish to thank J. Irwin and N. Duric for providing HI line and radio continuum images.

References

Beck, R., Golla, G. 1988, A&A 191, L9
Bicay M.D., Helou, G., 1990, ApJ 362, 59
Bicay, M.D., Helou, G., Condon, J.J. 1989, ApJ 338, L53
Bloemen, J.B.G.M., Deul, E.R., Thaddeus, P. 1990, A&A 233, 437
Boulanger, F., Pérault, M. 1988, ApJ 330, 964
Braine, J., Combes, F., Gerin, M. et al. 1993, A&AS 97, 887
Braine, J., Krügel, E., Sievers, A., Wielebinski, R. 1995, A&A 295 L55.
Cardelli, J.A., Meyer, D.M., Jura, M., Savage, B.D. 1996 ApJ 467, 334
Casoli, F., Combes, F., Dupraz, C., et al. 1988, A&A 192, L17
Chini, R., Kreysa, E., Krugel, E., & Mezger, P. G. 1986, A&A 166, L8
Chini, R., Krugel, E., Lemke, R., Ward-Thompson, D. 1995, A&A 295, 317
Condon, J.J. 1983, ApJS 53, 459.
Condon, J.J. 1987, ApJS 65, 485.
Condon, J.J., Anderson, M.L., Helou, G. 1991, ApJ 376, 95
Cox, P., Mezger, P.G. 1989, ARA&A 1, 49.
de Bruyn, A.G. 1977, A&A 58, 221
Dickman, R.L., Snell, R.L., Schloerb, F.P. 1986, ApJ 309, 326.
Dickey, J.M., Salpeter, E.E. 1984, ApJ 284 461
Downes, D., Solomon, P.M., Radford, S.J.E. 1993, ApJ 414, L13
Draine, B.T., Lee, H.M. 1984, ApJ 285, 89
Dumke, M., Braine, J., Krause, M. et al. 1997, A&A in press
Duric, N., Seaquist, E.R. 1988, ApJ 326, 574.
Eales, S.A., Wynn-Williams, C.G., Duncan, W.D. 1989, ApJ 339, 859
Filippenko, A.V., Sargent, W.L.W. 1992, AJ 103, 28
Ford, H.C., Dahari, O., Jacoby, G.H., Crane, P.C., Ciardullo, R. 1986, ApJ 311, L7
Gioia, I.M., Gregorini, L. 1980, A&AS 41, 329
Goldsmith, P., Bergin, E.A, Lis, D.C. 1995, IAU Symposium 170, CO: 25 Years of Millimeter-wave Spectroscopy
Guélin, M., Zylka, R., Mezger, P.G. et al. 1993, A&A 279, L37
Guélin, M., Zylka, R., Mezger, P.G. Haslam, C.G.T., Kreysa, E. 1993, A&A 298, L29
Hawarden, T.G., Israel, F.P., Geballe, T.R., Wade, R. 1995, MNRAS 276, 1197
Heckman, T.M., Armus, L., Miley, G.K. 1990, ApJS 74, 833
Hildebrand, R.H. 1983, QJRAS 24, 267
Hummel, E., van Gorkom, J.H. and Kotanyi, C. G. 1983, ApJ 267, L5.
Irwin, J.A., Sofue, Y., 1992, ApJ 396, L75
Irwin, J.A., Seaquist, E.R. 1991, ApJ 371 111.
Israel, F.P., van der Hulst, J.M. 1983, AJ 88, 1736
Kreysa, E. et al. 1993, in 4th Symposium on Space THz Technology, Los Angeles.
Krügel, E., Chini, R. 1994, A&A 287, 947.
Krügel, E. Siebenmorgen, R. 1994, A&A 288, 929
Léger, A., Jura, M., Omont, A. 1985, A&A 144, 147
Mathis, J.S., Rumpl, W., Nordsieck, K.H. 1977, ApJ 217, 425
Mathis, J.S., 1996 ApJ in press (UWM preprint 609)
Mauersberger, R., Henkel, C., Wielebinski, R., Wiklind, T., Reuter H.-P. 1996, A&A 305, 421
Mezger, P.G., Wink, J., Zylka, R. 1990, A&A 228, 95.
Neininger, N., Guélin, M., García-Burillo, S., Zy lka, R., Wielebinski, R. 1996, A&A 310, 725
Niklas, S. Klein, U., Braine, J., Wielebinski, R. 1995, A&AS 114, 21
Ossenkopf, V., Henning, T., 1994, A&A 291, 943
Pajot, F., Boissé, P., Gispert, R. et al. 1986, A&A 157, 393
Pajot, F.,Gispert, R., Lamarre, J.M. et al. 1989, A&A 223, 107
Pollack, J.B., Hollenbach, D., Beckwith, S. et al. 1994, ApJ 421, 615
Radford, S.J.E., Solomon, P.M., Downes, D., 1991, ApJ 368, L15
Reichert, G.A., Mushotsky, R.F., Filippenko, A.V. 1994, in Mass-Transfer Induced Activity in Galaxies de. I. Shlosman (Cambridge: Cambridge Univ. Press) p. 302
Rengarajan, T.N. 1984, A&A 140, 213
Rice, W., Boulanger, F., Viallefond, F., Soifer, B.T., Freedman, W.L. 1990, ApJ 358, 418
Richardson, K.M., Wolfendale, A.W. 1988, A&A 203, 289
Sandage, A., Tammann G.A. 1981, A Revised Shapley-Ames Catalog of Bright Galaxies (Washington D.C.: Carnegie Institute of Washington)

Scoville, N.Z., Sargent, A.I., Sanders, D.B., Soifer, B.T. 1991, ApJ 366, L5
Seaquist, E.R., Davis, L., Bignell, R.C. 1978, A&A 63, 199
Shier, L.M., Rieke, M.J., Rieke, G.H. 1994, ApJ 433, L9
Shostak, G.L. 1978, A&A 68, 321
Sievers, A.W., Reuter, H.-P., Haslam, C.G.T., Kreysa, E., Lemke, R. 1994, A&A 281, 681
Sodroski, T.J., Bennett, C., Boggess, N. et al. 1994, ApJ 428, 638
Sodroski, T.J., Odegard, N., Dwek, E. et al. 1995, ApJ 452, 262
Sofia, U.J., Cardelli, J.A., Savage, B.D. 1994, ApJ 430, 650
Solomon, P.M., Rivolo, A.R., Barrett, J., Yahil, A. 1987, ApJ 319, 730.
Solomon, P.M., Downes, D., Radford, S.J.E, Barrett, J.W., 1997, ApJ 478, 144
Strong, A.W., Bloemen, J.B.G.M., Dame, T.M. et al. 1988, A&A 207, 1
Sturm, E., Lutz, D., Genzel, R. et al. 1996, A&A 315, L133
Tacconi, L., Downes, D. in prep.
de Vaucouleurs, G., de Vaucouleurs, A., Corwin, H.G. et al. 1991, Third Reference Catalogue of Bright Galaxies, Springer-Verlag, New York. (RC3)
Veilleux, S., Cecil, G., Bland-Hawthorn, J. 1995, ApJ 445, 152
Walmsley, M. 1991, in Fragmentation of Molecular Clouds and Star Formation, p. 161, eds. E. Falgarone et al. IAU 147
Wild, W., Harris, A.I., Eckart, A. et al. 1992, A&A 265, 447
Young, J.S., Schloerb, F.P., Kenney, J., Lord, S.D. 1986, ApJ 304, 443.
Young, J. S., Xie, S., Kenney, J.D.P., Rice, W.L. 1989 ApJS 70 699

This article was processed by the author using Springer-Verlag LaTeX A&A style file *L-AA* version 3.